2023 FINESST Progress Report: Stellar Occultation Studies of Saturn's Atmosphere

March 15, 2023

Abstract

I started grad school in Fall 2016. I settled on an advisor and began scoping out and understanding this project in the Fall of 2018. In the Spring of 2019, I applied for and was awarded this grant over the Summer. I began work in the Fall of 2019. During that time, I created a preliminary analysis of the imaging-mode occultations as a launchpad for the rest of the analysis. In January of 2020, I put the grant on hiatus to help an emergency management start up. The grant resumed in 20 August 2022. I have been reacquainting myself with the field of astronomy, my skills in physics, and my previous work. This progress report represents my analysis of the work that I did during this grant's previous active period, my plans to complete the promised analysis of the Cassini VIMS occultation data per my proposal, and a discussion of planned publications using these data to constrain models of Saturn's atmospheric chemistry.

1 Administrative

Title of Grant: Stellar Occultation Studies of Saturn's Atmosphere
Name of Recipient on Grant: Andrew Scott Dickson Foster
Recipient's Preferred Name: An
Type of Report: Progress Report
Name of the principal investigator: Philip Nicholson
Period Covered by the report: 2022-08-20 to 2023-03-15
Cornell University, 418 Space Sciences Building, Ithaca, NY 14853
Grant Number: 80NSSC19K1528

2 Data Analysis: Objectives and Accomplishments

During the 13-year Cassini mission, the spacecraft observed over 100 occultations of stars by Saturn using the Visual and Infrared Mapping Spectrometer (VIMS) instrument. These occultations probe Saturn's atmosphere between pressures of ≈20 μbar and ≈5 mbar. Extinction of light from these stars is driven primarily by differential refraction and molecular

absorption by hydrocarbons (chiefly CH_4 and C_2H_6). We have proposed to tackle three scientific projects using these data: (1) to verify the seasonal and latitudinal temperature maps of Saturn's stratosphere generated by the Cassini Composite Infrared Spectrometer (CIRS) by Fletcher et al., 2007 at higher radial resolution, (2) to measure the altitude of the methane homopause from the dropoff of methane abundance with altitude, and (3) to test theoretical models of Saturn's photochemistry and eddy-diffusion rates (Moses and Greathouse, 2005). Our results for Saturn's atmosphere should complement similar analyses of VIMS solar occultation data for Titan by Maltagliati et al. (2015) and Bellucci et al. (2009).

A handful of these ≈100 occultation observations were observed through a series of small-frame images instead of a single spatial pixel pointed at the star's initial location on the sky. These imaging-mode occultations provide a chance to directly observe the stars' refraction through the outer layers of Saturn's atmosphere and constrain the relative importance of differential refraction to other sources of attenuation in the photometry of an occultation. This is an important calibration for the higher-radial-resolution occultation-mode data, for which the image of the star much more quickly gets refracted out of the field of view.

As such, my initial analysis targeted these imaging-mode occultations. I wrote a code that looks like Figure 1. It corrects out known sources of noise and performs standard aperture photometery. It produces lightcurves, X and Z centering results to track the star getting refracted out of frame, differences in the star's center by wavelength, spectra, and movies of these properties during the event. An example can be seen in Figure 2

There are four major tasks of the code, corresponding to the sections 2.1-2.4 below. 2.1-2.2 have been implemented in some form, and are iterating towards completion. These two act on only the imaging-mode data. 2.4-2.5 act on all data.

2.1 Background Subtraction

The standard aperture photometry methods employed are insufficient for these data. There isn't always a "sky", and the background level changes as the limb of the planet enters and then engulfs the field of view. The current method marks all pixels that the star appears in at any point of the occultation as part of the aperture, and the rest of the image as the sky. This is done because of how few pixels are available (64) and the large number of pixels occupied by the star as it is refracted across the detector (≈20 for some occultations). Multiple methods have been employed to remove time-dependent and spatial-dependent variations from these background corrections, as outlined in Figure 1. A more honest background correction needs to model this moving limb of the planet as having a different background flux for each frame's background correction. Discussions on implementing this have begun. For now, we are not yet ready to describe the new background correction in detail. Once this background correction is applied, the current version of the code sums all pixels in the oversized aperture to calculate stellar flux. The new version will use the Pixel Response Function scans described in the next section to estimate a more accurate total flux from the star, including the starlight that falls between pixels.

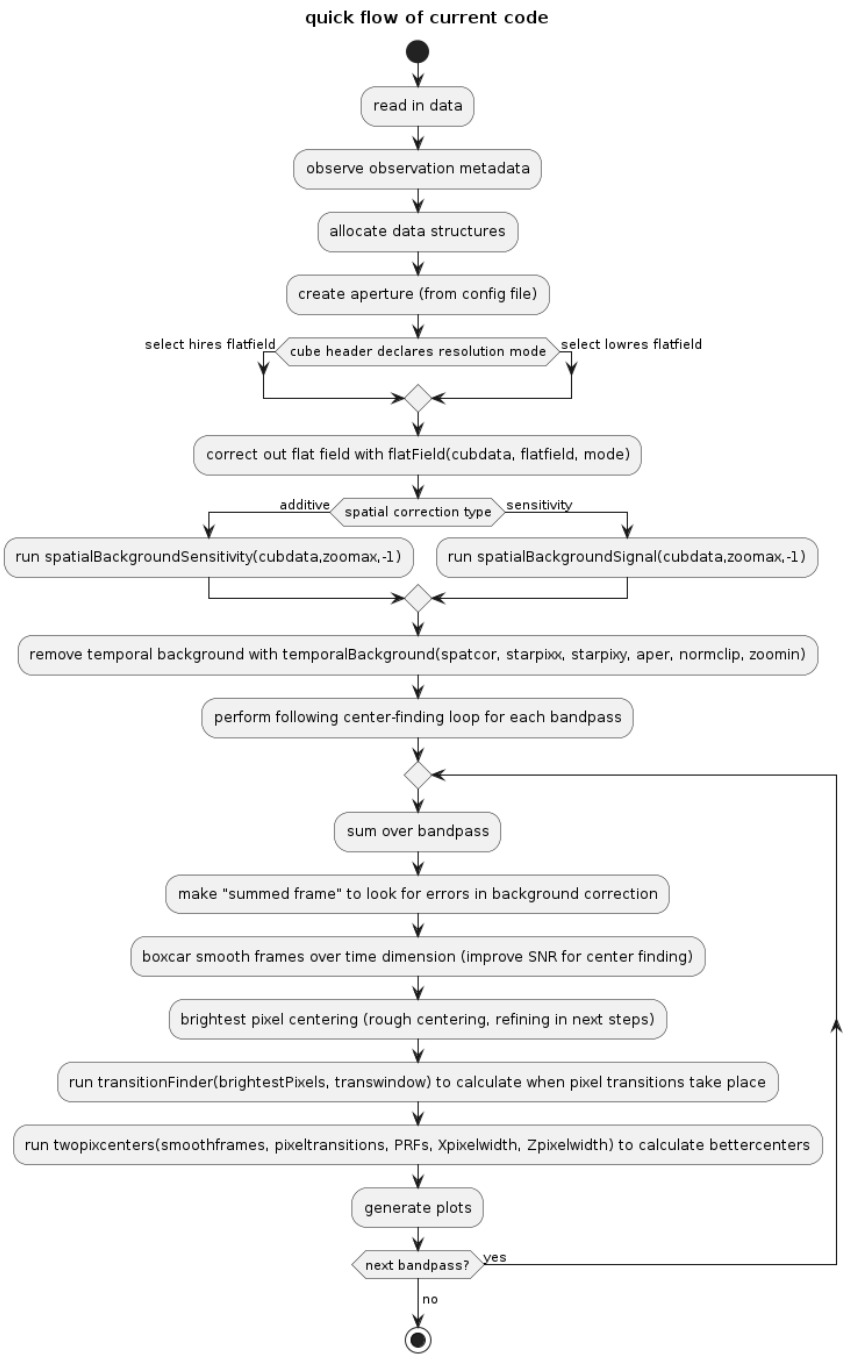

Figure 1: code flowchart for current version

2.2 Centering Algorithm

Tracking the center of a star in a VIMS image is a difficult task because the PSF of the star is less than one pixel. Still, the star is rarely centered in a pixel, and so centering can be achieved by looking at how much light spills into the neighbors of the brightest pixel. Fortunately, the Pixel Response Function (PRF) is well-defined for the single VIMS spatial

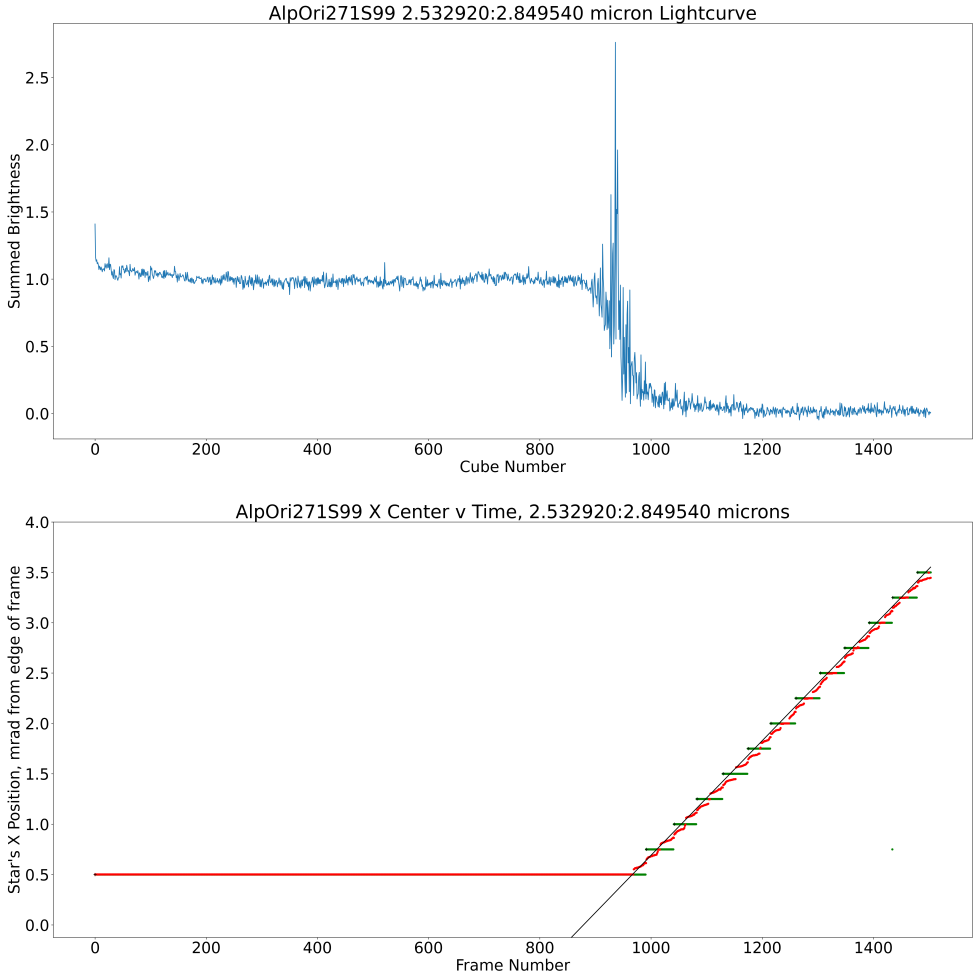

Figure 2: Lightcurve and centering results for an occultation of AlpOri (Betelgeuse) on orbit 271, observed in the 2.7 μm continuum band. The top plot displays the flux dropping and twinkling through the atmosphere. The bottom plot displays the pixel that the majority of starlight in (green), subpixel centering using the light spilling into a neighboring pixel (red), and a comparison with a line of slope matching the spacecraft's velocity perpendicular to the planet's limb (black). This is one of four types of plots produced by the code.

pixel as a function of the angle between the center of the pixel and the star. This has been done by slewing the spacecraft so that the star AlpOri (Betelgeuse) raster-scans across the pixel. From these, we can calculate the theoretical relative brightnesses of the pixels on either side of the brightest pixel relative to the brightest pixel, and compare this to the measured value in the VIMS frame.

First, we must determine which two pixels share the most starlight. To do so, we:

1. integrate over a continuum bandpass to improve signal to noise (e.g. 2.53-2.85 microns)
2. perform a boxcar smoothing in time (usually 10 frames)
3. record the brightest pixel for each resulting timestep
4. locate "transition times" when the brightest pixel changes from one timestep to the next
5. at each timestep select the brightest pixel and the brightest pixel on the other side of the nearest "transition"

We measure the direction to the star by taking the ratio (R_{data}) of the measured flux in these two selected pixels. We compare this ratio to the same ratio calculated from the PRF scans $R_{scans}(t)$ at each time step t. We calculate the value of $t = t_0$ for which $\chi^2 = (R_{data} - R_{scans}(t_0))^2$ is minimized, and then calculate $\theta(t_0)$ which is the offset of the star from the center of the pixel at t_0.

This metric has many properties which make it useful. Theoretically, it should be monotonically increasing or decreasing as the star moves steadily in pixel position. For PSFs smaller than a pixel, there will be a plateau at zero where there is no light observed in the neighboring pixel. Away from this plateau (near the pixel boundaries) we have the best sensitivity to the position of the star. At metric values $R = 1$ the center of the star's PSF straddles the boundary with the neighboring pixel and we have the most sensitivity.

The current version of the code performs fits in each direction independently, and using manually-selected PRF scan track numbers. A planned improvement is to fit both simultaneously, which will allow the algorithm to self-select the best track for each direction.

After this step, we have occultation profiles in the same form as the occultation-mode data. This ends the imaging-mode specific portion of the code. The following two subsections describe code that will be run on all occultation data.

2.3 Calculating Temperature and Pressure from Refraction in the Continuum Bands

The current version of the code does not yet perform this calculation.

Consider a light ray from the occulted star incident on a spherical planet of radius R, at an impact parameter ρ. As it penetrates more deeply into the atmosphere, where the refractive index of the gas is larger, the ray gradually refracts towards the planet's center until it reaches a minimum radius, after which it traces a mirror-image path back out of the atmosphere.

The formal expression for the overall angular deflection of the ray once it emerges from the atmosphere is:

$$\theta(\rho) = -2\rho \int_{r_0}^{\infty} \frac{dn/dr}{n\sqrt{n^2 r^2 - \rho^2}}\, dr, \tag{1}$$

where $n(r)$ is the refractive index profile of the atmosphere, and the ray's minimum radius r_0 is specified by the condition $n(r_0)r_0 = \rho$.

Adjacent light rays are deflected by progressively larger amounts as ρ decreases and the rays penetrate more deeply into the atmosphere. As a result of this *differential refraction*, the flux of light from the source is reduced by a factor of Φ:

$$\Phi(\rho) = \left(1 - D\frac{d\theta}{d\rho}\right)^{-1} \left(1 - \frac{D\theta}{\rho}\right)^{-1}, \tag{2}$$

where D is the distance from the planet to the observer. The second factor represents the focusing effect that occurs near the center of the geometric shadow and can be neglected for our data where $D\theta \ll \rho$.

As described in Elliot et al. (1977) and French et al. (1978), we can use these two expressions to perform an inverse Abel transform and invert our occultation lightcurves in regions of the spectra dominated by differential refraction to acquire multiple **radial profiles of refractive index, density, and thence the temperature and pressure in the planet's stratosphere.**

This technique is standard for inversions of differential-refraction dominated stellar occultations. Due to Saturn's highly oblate shape, the above expressions are adjusted in practice to use a local spherical fit to the atmosphere.

We are confident that the attenuation of the starlight at wavelengths where hydrocarbon molecular absorption is negligible is dominated by the above-described impact of differential refraction and not aerosol-driven scattering extinction. Although aerosols are an important chemical component of Saturn's atmosphere, these particles are likely sub-micron in size and their scattering efficiency should decrease rapidly with increasing wavelength, perhaps scaling as λ^{-q} where q is between 1 and 4. The aerosols on Titan follow such a power law with $q \simeq 1.8 \pm 0.5$ (Bellucci et al., 2009). The extinction in the VIMS Saturn occultations at wavelengths outside of the strong hydrocarbon bands is observed to be essentially *independent* of wavelength, strongly suggesting that aerosol extinction is negligible at the few mbar level and above and therefore we may neglect them in our models. **One goal of the imaging-mode occultations is to test this assumption by following the star much deeper into the occultation than is available in occultation-mode, and directly measuring the bending angle (distance the image has moved across the detector) and the flux to compare to values predicted by the above equations.**

2.4 Calculating Molecular Abundances from Spectra

The current version of the code does not yet perform this calculation.

Let's consider an "onion-skin" model of an atmosphere for which each thin radial layer is of uniform composition and density. As a ray of star light passes through each of these layers, it is attenuated according to the equation:

$$\Phi(\lambda) = \Phi_0 \; e^{-\delta\tau(\lambda)}, \tag{3}$$

where Φ_0 is the attenuation experienced before entering that layer and $\delta\tau(\lambda)$ is the optical depth of the layer as a function of wavelength, described by the equation:

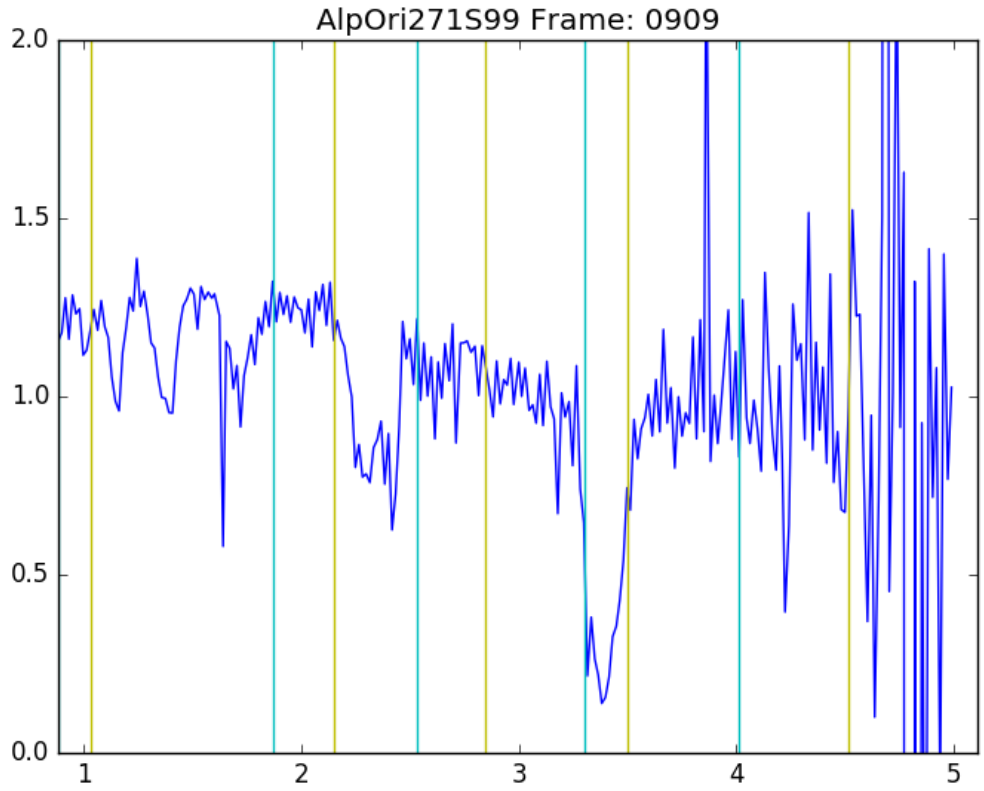

Figure 3: Saturn stratospheric absorption spectrum sample. VIMS spectra cover the range 1-5μm, but with signal fairly poor for most stars beyond $\approx 4\mu$m. In the spectrum, we can see clear hydrocarbon absorption features at 3.4μm, 2.3μm, 1.7μm, and 1.2μm. These features correspond to absorption frequencies of CH_4 and C_2H_6. These two molecules have similar spectra at this resolution, but C_2H_6's 2.3μm feature is stronger and broader than CH_4's. The VIMS-IR spectral resolution is 0.017 μm, which is quite low by atmospheric standards. We cannot discern individual lines in these data, just broad bands. The vertical lines in this figure represent the boundaries of frequency bands being summed and studied during a preliminary analysis.

$$\delta\tau(\lambda) = \kappa(\lambda)Ld \tag{4}$$

Here, κ is the absorption coefficient, L is the slant pathlength, and d is the density of the layer which is known from the inversion of the lightcurve at the refraction-dominated continuum wavelengths.

The data for a given occultation can be thought of as a time-series of spectra, each of which cuts a deeper path through the atmosphere than its predecessor. Each time-step can be used to constrain the opacity of an additional deeper layer, and then be used as an input to the next timestep since that layer will also be probed during the subsequent observations. Datapoints can be binned in time to increase signal to noise at the expense of the radial

resolution of the resulting abundance profile. We call this technique "onion-peeling" and a preliminary proof-of-concept using a single wavelength bin was presented by Banfield et al. (2011).

We will fit a model to a full-spectrum $\kappa(\lambda)$ calculated in each layer from our data. A model spectrum will be calculated with a line-by-line approach using Voigt profiles calculated using the pressures and temperatures from our refraction inversions described above. We will use line list databases such as the HITEMP database from HITRAN [1] (Gordon et al., 2017) for each gas relevant to Saturn's atmosphere. The contributions of each gas (chiefly CH_4 and C_2H_6, but possibly also C_2H_2) to the final opacity are independent and proportional to their mixing ratios, which will be fit to the data.

In practice, hydrogen and helium are essentially transparent in the near-infrared for any reasonable path length through the stratosphere [2] so the opacity is dominated by trace gases, methane, ethane, and acetylene (Moses and Greathouse, 2005).

This is supported by preliminary spectra produced for the image-mode occultations which show a clear hydrocarbon absorption spectrum. An example spectrum can be found in Figure 3.

3 Budget Changes

No changes to report

4 Dissemination of Results

No publications or conference presentations during this period.

References

Banfield, D., Gierasch, P. J., Conrath, B. J., Nicholson, P. D., Hedman, M. M. 2011. Saturn's He and CH4 Abundances from Cassini VIMS Occultations & CIRS Limb Spectra. EPSC-DPS Joint Meeting 2011 1548.

Bellucci, A., Sicardy, B., Drossart, P., Rannou, P., Nicholson, P. D., Hedman, M., Baines, K. H., Burrati, B. 2009. Titan solar occultation observed by Cassini/VIMS: Gas absorption and constraints on aerosol composition. Icarus 201, 198-216.

Elliot, J. L., French, R. G., Dunham, E., Gierasch, P. J., Veverka, J., Church, C., Sagan, C. 1977. Occultation of Epsilon Geminorum by Mars. II - The structure and extinction of the Martian upper atmosphere. The Astrophysical Journal 217, 661-679.

[1] https://hitran.org/hitemp

[2] H_2 does have a fundamental vibrational transition at 2.1 μm, which is detectable in the spectra of the Jovian planets, but this is a collision-induced absorption that scales as p^2, and so is very weak in the stratosphere, even for very long path lengths.

Fletcher, L. N. and Irwin, P. G. J. and Teanby, N. A. and Orton, G. S. and Parrish, P. D. and de Kok, R. and Howett, C. and Calcutt, S. B. and Bowles, N. and Taylor, F. W., 2007 Characterising Saturn's Vertical Temperature Structure from Cassini/CIRS Icarus 189, 457-478.

French, R. G., Elliot, J. L., Gierasch, P. J. 1978. Analysis of stellar occultation data - Effects of photon noise and initial conditions. Icarus 33, 186-202.

Gordon, I. E. Rothman, L. S. Hill, C. 2017. The HITRAN2016 Molecular Spectroscopic Database Journal of Quantitative Spectroscopy and Radiative Transfer 203, 3-69.

Moses, J. I., Greathouse, T. K. 2005. Latitudinal and seasonal models of stratospheric photochemistry on Saturn: Comparison with infrared data from IRTF/TEXES. Journal of Geophysical Research (Planets) 110, E09007.